# Towards highly efficient continuous-flow catalytic carbon dioxide cycloadditions with additively manufactured reactors

David Valverde,[a] Raúl Porcar, [a,b] Marcileia Zanatta,[c] Sergio Alcalde,[a] Belen Altava,[a] Victor Sans,*[c] Eduardo García-Verdugo *[a]

[a] Departamento de Química Inorgánica y Orgánica, Grupo de Química Sostenible y Supramolecular Universidad Jaume I, E-12071 Castellón, Spain
[b] Departamento de Química Orgánica y Bio-Orgánica, Facultad de Ciencias, UNED, Avenida de Esparta s/n, 28232. Las Rozas-Madrid, Spain
[c] Institute of Advanced Materials (INAM), Univesitat Jaume I, Avda Sos Baynat s/n, 12071, Castellón, Spain

*cepeda@uji.es, sans@uji.es*

**Abstract.** Developing efficient and sustainable methodologies to transform $CO_2$ into added value chemicals is an important strategy to decarbonize the chemical industry. Here, a new multi-scale approach for the cycloaddition of $CO_2$ to epoxides is reported, combining by design hydrogen bond ability, metal-free catalysts and supported ionic liquids on polymers. The use of additive manufacturing (AM) techniques allowed the digital design and rapid fabrication of structured architectures for continuous-flow reactors, which offers potential for process optimization. AM generated catalytic reactors showed higher catalytic activity than similar sized packed bed reactors, when normalised to the amount of catalyst and their surface area. The catalytic activity and stability were maintained over a prolonged period of time (300 h) without loss of activity, and it was demonstrated to efficiently transform a range of epoxide substrates.

**Keywords:** 3D printing • Supported Ionic Liquids • catalysis • $CO_2$ conversion • flow chemistry

## Introduction

Chemical fixation of carbon dioxide ($CO_2$) into valuable chemicals and fuels has attracted great attention in recent years due to environmental and climate change concerns, and to the perspective of having access to an abundant and cheap C1 building block.[1] The reuse of $CO_2$ to produce cyclic carbonates have emerged as an alternative, since they are commonly used as intermediate for the synthesis of polycarbonates and polyurethanes, organic solvents, electrolytes in the Li-ion battery, and in cosmetic and pharmaceutical preparations. This reaction is exergonic, but it requires activation with a catalyst to proceed efficiently. In this context, considerable progress has been made to create selective, active, and highly efficient homogeneous and heterogeneous catalysts.[2-4] However, the development of continuous-flow scalable systems for these processes is still in its infancy, generating a gap between academic and industrial protocols.[5-8] Compared to batch systems, continuous-flow catalytic systems allow to improve mixing, manage heat transfer more efficiently, increase catalytic performance by improving the contact between the phases, increase productivity by continuously adding reagents and removing products from the reactor and generally speaking provide a more reproducible, scalable, safe and efficient option for performing chemical reactions, which represent an industrially attractive technology.[9-13]

The design and manufacture of efficient and scalable catalytic reactors is highly challenging.[14] Indeed, the fabrication of fixed-bed catalytic reactors face several challenges to balance process efficiency with mass and heat transport limitations. Within this context, additive manufacturing (AM), commonly known as 3D printing (3DP) is a set of emerging technologies that facilitates the generation of complex geometries in a variety of materials (i.e. polymers, ceramics and metals).[15-17] Microstereolithography (MSLA) of photocurable resins offers a great potential to develop advanced designs for continuous-flow processing.[18] The high resolution and the flexibility to formulate a broad range of materials are key advantages of this technique. Recently, it has been demonstrated the possibility to fabricate large structures in a rapid and efficient fashion, thus opening the door for future scale-up to industrial scale.[19] Several examples of AM based continuous-flow reactors to perform synthetic transformations have appeared in the literature in recent years.[18, 20-25]

Ionic liquids (ILs) have demonstrated to be efficient catalytic media for $CO_2$ cycloaddition reactions.[26, 27] The effective immobilization of ILs by grafting ILs units onto supported polymeric matrices, called from here onwards Supported ionic liquids (SILs) enables the efficient transfer of IL properties to active surfaces.[28, 29] Furthermore, the crosslinked polymeric backbones offer an additional design vector to optimize their macroscopic properties for a given process.[30] This facilitates the separation, recover and reutilization of both the catalyst and the IL phase in subsequent reaction cycles. The combination of SILs and AM technologies enables the creation of devices capable of highly sophisticated functional operations for advanced applications, including information storage,[31] antimicrobials[32] and catalysis.[33] The development of catalytic applications of SILs under continuous-flow offers a broad range of opportunities for sustainable manufacturing.[11, 34-40]

Here, we report our efforts to integrate design across the scales to generate highly efficient continuous-flow catalytic reactors for $CO_2$ cycloadditions (Figure 1). New formulations compatible with MSLA have been developed. Simple post-functionalization by grafting generated highly efficient catalytic systems that conveniently combine IL with hydrogen bond donor species. The special design of the materials processed by AM is the key to integrate and transfer the optimised characteristic of the ILs at the molecular level to materials and macroscale devices able to efficiently convert $CO_2$ under continuous-flow. The data presented here suggests that the digital design of the reactor has a significant influence on the catalytic performance observed. Furthermore, an AM-based reactor demonstrated higher normalised activity than a packed-bed column based on the use of commercially available materials with similar formulation.
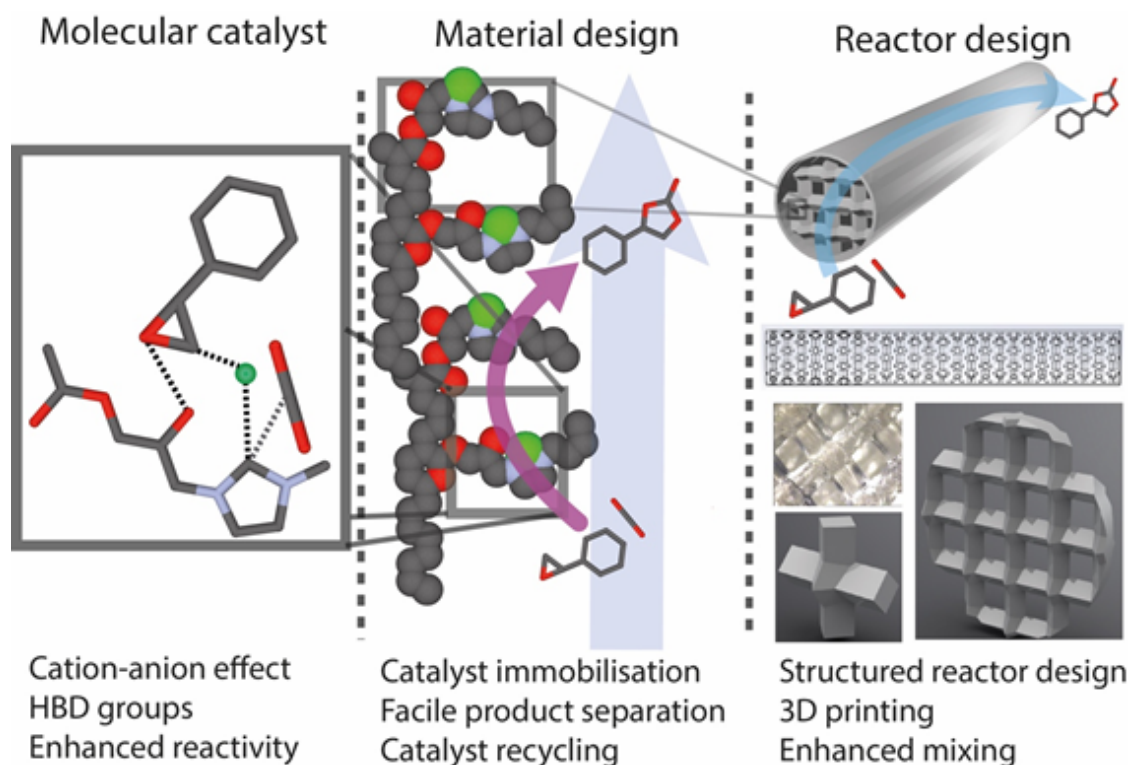
**Figure 1.** Conceptual framework of design across scales presented in this work. Highly efficient molecular catalysts based on the combination of hydrogen bonding and anion-based catalysis is integrated in polymer networks. The polymeric precursors can be 3D printed into structured reactors with optimal flow dynamics.

## Results and Discussion

In the search for a straightforward and simple methodology for the preparation of functionalised AM polymeric devices, the commercial monomer glycidyl methacrylate (GMA) was envisioned as a suitable functional monomer. GMA copolymerizes with many conventional monomers and offers an economical means to introduce reactive functional groups into polymeric matrices, facilitating the polymer post-functionalisation for different applications.[41, 42] In this context, two different types of monomeric mixtures have been used to produce functional polymeric materials by AM in presence of phenylbis(2,4,6-trimethylbenzoyl)-phosphine) oxide (BAPO) as the photoinitiator: *(i)* formed by GMA and commercially available AM ink in absence of any additional crosslinker (named support **S0**, Table S1). Commercial acrylate-based resin (Elegoo Clear resin™) was

employed as an additive (10%wt) to improve polymerization kinetics and mechanical properties of the materials; and *(ii)* in the presence of additional acrylate-based crosslinker (named support **S1** and **S2**) (Figure 2A and Table S2). The additional cross-linkers were used to assess the effect of the polymeric backbone and to finely tune the mechanical properties of the final materials. Two different methacrylate-based compounds were tested as additional crosslinkers: ethylene glycol dimethacrylate (EGDMA) (**S1 a-h**, entries 1-8, Table S2) and poly(ethylene glycol) dimethacrylate with an average $M_n$ of 250 (PEGDMA-250), (**S1 i-p**, entries 9-16, Table S2). A subsequent generation with a more reactive cross-linker, 1,4-Butanediol diacrylate (1,4-BUDA) (**S2,** entry 17, Table S2) allowed the efficient photopolymerization under conditions compatible with the printers employed without the requirement of any additional additive. The obtained materials were exposed to different organic solvents and styrene oxide to evaluate their degree of swelling and chemical stability (Table S2-S5). It should be noted that all polymerisations were performed under bulk conditions without addition of any porogenic agent. Thus, it is expected that these polymeric devices will not present a permanent porosity. However, they can swell under the action of compatible solvents or reagents.[43] A high degree of swelling is not recommendable for 3D structures obtained by AM for the applications considered here, as they will experiment significant volume changes, which are not optimal for continuous-flow applications.[44] The swelling degree can be controlled by the amount of cross-linker. Thus, different polymerisation mixtures containing a fixed amount of commercially available 3DP ink (10% w/w, see SI for more detail), different ratios of GMA and an additional crosslinking agent were assayed (Table S2). The increase of the crosslinking help to enhance the mechanical stability polymeric materials, while reducing the swelling. From all the compositions tested using methacrylate-based crosslinkers, **S1.g** was selected for the following steps because it showed lower degree of swelling and good mechanical stability (Entry 7, Table S2). Furthermore, from these preliminary results, a final optimized formulation using 1,4-BUDA as crosslinker instead of EGDMA, named **S2** (Entry 17, Table S2), allowed to print devices in the absence of commercial photopolymer resin. This material also presented low swelling degree and good mechanical stability, resulting in a good alternative to be further used to print devices (see 3DP tests Figures S1-S2).
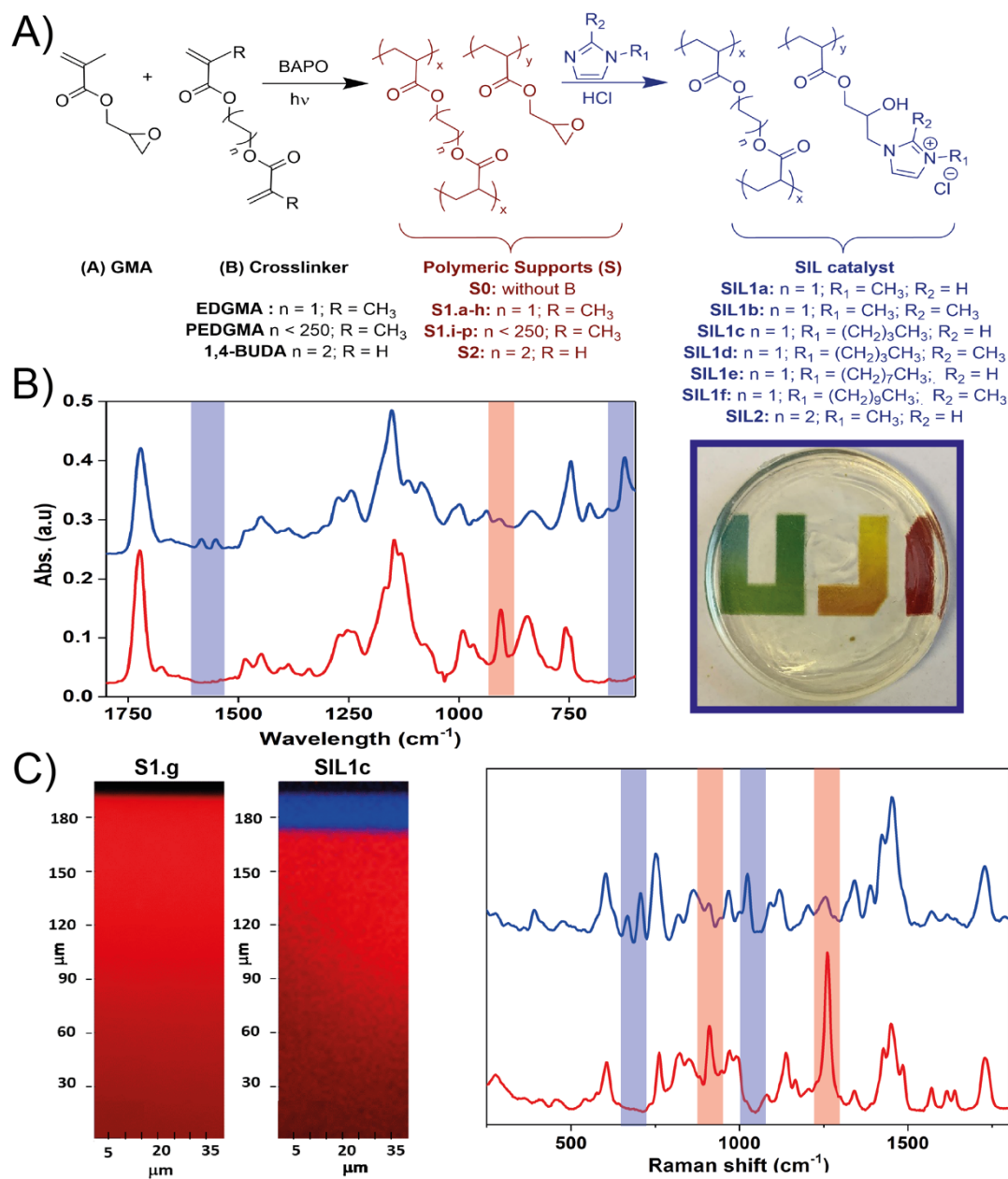
Figure 2. **A) SIL** preparation. First reaction: polymerization reaction to prepare epoxy support (**S0-2** in red); Second reaction: functionalization of epoxy support with different N-alkyl-imidazoles IL, resulting in **SIL** materials (in blue); **B)** *Left:* FT-IR-ATR of the polymeric support **S1.g** before (in red) and after (in blue) imidazolium functionalization (**SI Figure 2**). *Right:* Picture of the resulting polymeric discs. *c)* Raman confocal microscopy study of **S1.g** and **SIL1.c**. **C)**. *Left)* Mapping for the initial 200 μm depth of the disc: black region corresponds to air, the blue region corresponds to the surface modification with imidazolium units, the red region corresponds to the unmodified epoxy region. *Right)* Raman spectra corresponding to the blue (surface) and red (core polymer) regions.

**S1.g** and **S2** were selected to proceed with the functionalization through the nucleophilic ring opening of the epoxides in presence of the chloride salt of different N-alkyl-imidazole,[45] generating the **SIL1** and **SIL2**, respectively. For **SIL1**, different imidazolium alkyl chains were used: methyl-, butyl, octyl- and 1-decyl-2-methyl- (Table S6). The modification was monitored by FT-ATR-IR (Figure 2B and S3) shows the spectra of the polymer before (**S1.g**) and after functionalization (**SIL1**). The opening of the epoxy ring was confirmed by the appearance of a peak associated with OH stretching at 3273 cm$^{-1}$ and the almost complete disappearance of the peak at 905 cm$^{-1}$, corresponding to the C-O stretching of the epoxide (Figure S3b). The spectra also showed the presence of new peaks related to the imidazolium moiety at 3146 and 3111 cm$^{-1}$ assigned to $C_2$–H stretching (low frequency component) and $C_{4,5}$–H stretching (high frequency component) together with signals at 1584 cm$^{-1}$ and 1551 cm$^{-1}$ (C=N ring stretching), 907 cm$^{-1}$ (C–C stretching) and at 700, 659 and 624 cm$^{-1}$ (out-of-plane ring vibrations) (Figure 2B and S3).[46] It should be noted that the penetration depth in the sample for FT-IR ATR experiments is typically between 0.5 and 2 µm, with the exact value determined by the wavelength of the light, the angle of incidence and the refraction indices of the ATR crystal and the medium being probed.[47] Thus, the data obtained from ATR spectroscopy only provided information about the modification of the surface. To identify the extension of the surface modification, Raman confocal microscopy analyses of the samples were performed. This technique allows mapping the composition of the polymer with a penetration depth of *ca*. 200 µm. Figure 2C shows the mapping obtained for the disc materials before (**S1.g**) and after modification with butyl imidazole (**SIL1.c**) (Figure 2C) using different penetrations for the incident laser light. This analysis confirmed functionalization is taking place only on the polymer surface. The Raman of the **S1.g** reveals the presence of a single component on the entire depth evaluated (red in Figure 2C). This main component, as expected, corresponds to the epoxy resin, with peaks at 1729 cm$^{-1}$ (C=O) characteristic of the ester group of the acrylic monomers and at 1261 cm$^{-1}$ and 911 cm$^{-1}$ assignable to the epoxy groups (asymmetric and symmetric stretching respectively).[48] However, the mapping of **SIL1.c** clearly shows the presence of two different and spatially separated components. From the figure is possible to observe three different regions: *(i)* the black region corresponds to air;

*(ii)* blue region corresponds to the surface modification with imidazolium units (**SIL**s); *(iii)* the red region corresponds to the unmodified epoxy region (Support). In addition, the Raman spectra of blue and red region of functionalized support **(SIL1.c)** can be seen in right part of Figure 2C. The analysis of the spectra of **SIL1.c** surface (thin layer of *ca*. 10 μm depth - in blue) reveals the appearance of new peaks at 1025 cm$^{-1}$ (C-H, in plane bending), 707 cm$^{-1}$ and 667 cm$^{-1}$ (C-C, out of plane ring vibrations) assignable to the imidazolium substitution, and a significant change in the of 1500-1300 cm$^{-1}$ region where the C=C and C=N bond stretching bands of imidazolium appear.[49] The Raman analysis of bulky polymer (in red) reveals the presence unmodified epoxy resin, with peaks above mentioned assignable to the epoxy groups. Hence, under the experimental conditions assayed, only a superficial modification of *ca* 10 μm depth of polymeric materials is achieved, which also explains the low loading of imidazolium units found by elemental analysis (Table 1). Indeed, these results are in good agreement with the expected non-porous nature of the polymeric devices obtained under bulk polymerisation in absence of any porogenic solvent. The modification of the surface was also confirmed by performing water contact angle measurements (WCA), since the wettability of a solid surface changes with the chemical composition of the IL moieties attached to the solid surfaces, see supporting information for more details (Figure S5).[50-55] Finally, the low swelling degree of the epoxy polymeric material in ethanol (entry 2, Table S3) is also likely to contribute low degree of functionality as only the superficial groups will be available at the surface of the material for modification. All these analyses suggest that the catalysis will occur only in the surface of material.

An initial catalytic screening was carried out by submerging **SIL1** catalysts in styrene oxide (SO) and pressurising the autoclave reactor with $CO_2$ at 10 bar and 100 ºC. As a control experiment, the reaction did not take place in absence of IL phase (Entry 1,

Table **1**). All the supported salts provided good conversions, with excellent selectivity (>99%), except in the case of methylimidazole (Entries 2-3,

Table **1**). A slight reduction in conversion was observed when the H in the C2 position of imidazolium ring (entries 2 and 4) with $CH_3$ ( entries 3 and 5,

Table **1**), similar to previously reported for imidazolium-based ILs.[56]. In this specific case, the presence of hydroxy groups in the IL structure may compensate the absence of H2 by helping the activation of the epoxide ring. [2, 57-59] The epoxide activation is the widely accepted mechanism for $CO_2$ cycloaddition to epoxide. The pathway requires a catalyst able to coordinate to the epoxide activating this substrate towards ring-opening by a nucleophile. For imidazolium-based IL, the hydrogens of the imidazolium generally play this role. In our specific case, the role of the imidazolium was presumably reinforced by the presence of hydroxy groups, which can activate the epoxide by hydrogen bond interactions, while the anion (Cl) works as a nucleophile. The resulting alkoxide intermediate then reacts with $CO_2$ to form a carbonate intermediate. The last step is the cyclisation to form the cyclic carbonate and regenerate the nucleophile and catalyst.[4]

In agreement with previous reports, the conversion of epoxide increased with the increases of length of the alkyl chain, from $C_1$ to $C_{10}$ (entries 2-7).[60, 61] Very interestingly, a control experiment using commercial polymeric beads (P-SIL - Purolite Lifetech™ ECR8209M) dried and modified with the same imidazolium moieties, instead of discs resulted in similar cyclic carbonate yield. However, the polymeric beads presenting higher molar amount of IL in the surface, showed a slight reduction in conversion from 88 to 91% (entries 8 and 4, respectively).

In addition, it is worth mentioning that the SIL developed in this work present better results when compared to polystyrene-divinylbenzene (PS-DVB)-derivatives (commercial Merrifield resin) containing Rose Bengal immobilized onto SIL (RB-SIL) previously reported by our group. In that work, using similar conditions, lower conversion (39%) was obtained even in the presence of a co-catalyst (63%). [62] The best results reported herein is attributed to the presence of a hydroxyl group in the alkyl chain of imidazolium, which increased the hydrogen bond donor ability of the catalyst.[63-66]

**Table 1.** Screening of SILs as catalysts in the reaction between SO and $CO_2$ to yield styrene carbonate.[a]
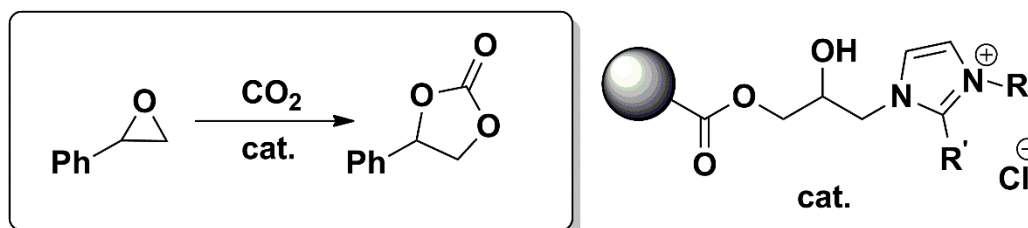


| Entry | Cat. | IL Loading[b] [mmol g$^{-1}$] | R | R′ | Conversion [c] [%] |
|-------|------|------|------|------|------|
| 1 | S1 | 0 | - | - | 0 |
| 2 | SIL1.a | 0.076 | $CH_3$ | H | 56 |
| 3 | SIL1.b | 0.075 | $CH_3$ | $CH_3$ | 49 |
| 4 | SIL1.c | 0.088 | $CH_3(CH_2)_3$ | H | 91 |
| 5 | SIL1.d | 0.087 | $CH_3(CH_2)_3$ | $CH_3$ | 82 |
| 6 | SIL1.e | 0.091 | $CH_3(CH_2)_7$ | H | 80 |
| 7 | SIL1.f | 0.071 | $CH_3(CH_2)_9$ | $CH_3$ | 86 |
| 8 | P-SIL[d] | 0.213 | $CH_3(CH_2)_3$ | H | 88 |

[a] solventless, 12 h, 100 ºC, 10 bar $CO_2$, 1 mL epoxide, 1.0g cat., without co-catalyst. [b] Imidazolium unit loading calculated by elemental analysis. [c] Calculated by ^{1}H-NMR. Selectivity >99.9%.[d] polymeric beads of commercially available resin (Purolite Lifetech™ ECR8209M) functionalised with methyl-imidazolium moieties

With the best catalyst moiety in hand (SIL1c), digital design of the structured reactor was employed with the aim to improve flow dynamics and therefore performance of the transformations. The relatively slow polymerization kinetics from S1 formulations required long irradiation times per layer (120 s), which in turn required printing two columns of 7.5 cm length, which were packed together in an Omnifit column. These structures can be accommodated in a commercially available Omnifit™ column (L: 15cm, Ø: 1.0cm) enabling their use under flow conditions (Figure 3). Figure 3A depict the two designs assayed. Based on the

repetition of this motif along the x-y axes, a grid structure with circular shape was generated, with a diameter adapted to the commercially available Omnifit columns. This structure was periodically repeated along a longitudinal axis at 3 mm intervals to generate a 3D structured reactor. Design 1 (**D1**) had a deviation in every second grid of 3 mm along the y axis to ensure the different phases had to be in intimate contact with the catalytic surfaces during the flow through the reactor. The design 2 (**D2**) was employed as a control experiment, where the grids were placed in a straight fashion, thus resulting in perfectly aligned along the longitudinal axis. Using the selected formulation, **SIL1.c** (Entry 4,

Table **1**), two monolithic designs were obtained without any obvious defects or inhomogeneity by AM, named **SIL1-D1** and **SIL1-D2** (Figure 3B-C).
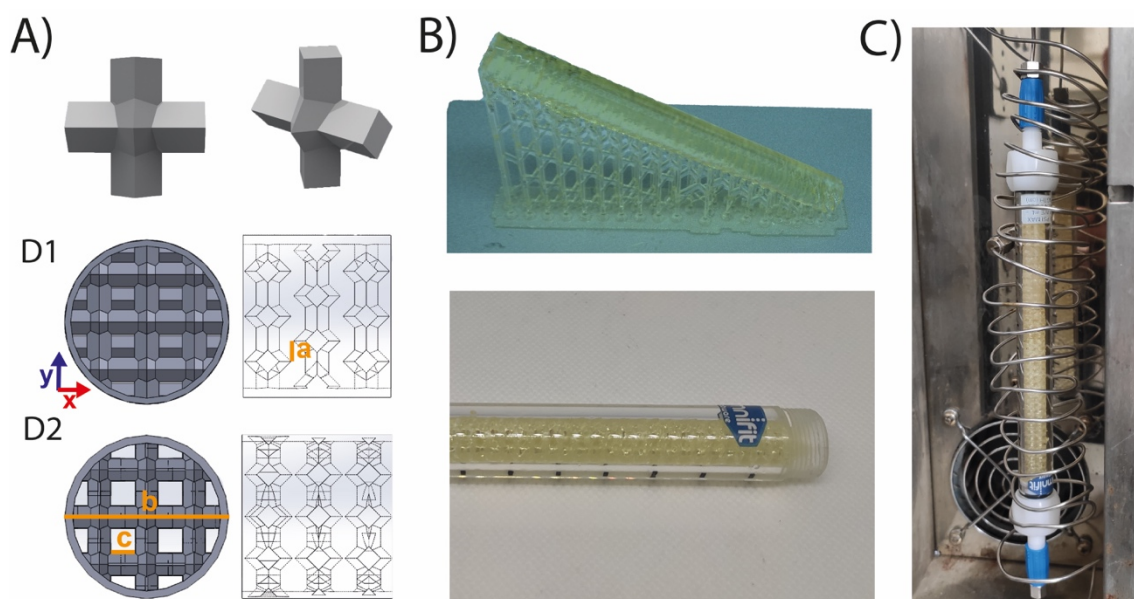


**Figure 3.** A) Computer-aided design (SolidWorks or CAD) of structured catalytic reactors. The building block units (up) were reproduced in cylindric grids and with periodic repetition across the length of the cylindric structure. Dx=a=4 mm; b= 0.95 cm; c=1.3 mm. For D1 d=3mm and for D2 d=4mm. B) Example of design D1 fabricated with m-SLA AM as obtained in the printer platform with supports (up) and accommodated in an Omnifit™ column. **C)** Omnifit™ column (L:15cm, Ø:1.0cm) holding the **SIL1-D1** and **SIL1-D2** for its application under flow conditions.

A continuous flow set-up was built as schematically shown in Figure 4. Two pumps were used to deliver $CO_2$ and the epoxide to a mixer, forming a homogeneous

mixture that then passes through a preheater to reach the reaction temperature before entering in contact with the supported catalyst. The reaction was performed using an oven temperature of 120 $^{\circ}$C under 20 bar of $CO_2$ pressure. Results were rather different depending on the monolithic design. The monolith **SIL1-D2** provided a yield of *ca*. 38%, while this value was increased to *ca*. 60% yield for **SIL1-D1**. It should be mentioned that both systems showed a remarkable stability without any activity deterioration, under flow conditions, during at least 5 days of continuous use.

In addition, since each structured reactor presents different amounts of catalyst and geometric surface area, it was necessary to normalise the results to enable a meaningful comparison between them. Catalyst loading was determined by elemental analysis, considering imidazolium unit as the active moiety. The reactor surface area was calculated based on the theoretical CAD design for the structured reactors (90 $cm^{-2}$ and 123 $cm^{-2}$ for D1 and D2 respectively). The PBR surface area was calculated based on BET results multiplied by the mass of polymer employed, yielding a total of 280 $cm^{-2}$. The productivity *vs* time on stream calculated in this way ($g_{prod}$ $mol_{cat}^{-1}$ $cm^{-2}$ $h^{-1}$) shows that, under the conditions employed, the performance can be significantly improved as a function of the reactor design. **SIL1-D1** achieved the highest values of conversion and productivity per imidazolium unit and reactor volume (*ca*. 3.2 *vs* 1.5 g of product · mol of imidazolium$^{-1}$ · $cm^{-2}$ · $h^{-1}$ for **SIL1-D1** and **SIL1-D2**, respectively). This can be explained by the more intricate design structure of **SIL1-D1**, which is likely to provide enhanced fluid dynamics and distribution of the gas and liquid phases facilitating the contact with the catalytic surfaces and leading to enhanced productivity in comparison with the **SIL1-D2** with simpler fluid dynamics.

Very interestingly, the productivity observed for **SIL1-D1** was superior to a packed-bed reactor (PBR) generated from spheric beads of **P-SIL1**, which is a commercially available resin (Purolite Lifetech™ ECR8209M) functionalised with methyl-imidazolium moieties. The PBR (Figure 4 in green) showed a productivity of 2.1 $g_{prod}$ $mol_{cat}^{-1}$ $cm^{-2}$ $h^{-1}$. This preliminary result clearly indicates the influence of reactor architecture in the reaction conversion and productivity, reinforcing the key role of 3D printing in design of reactors. Further optimization of the ink

formulation would lead to improved higher printing resolution, that will allow to develop more intricate reactor geometries, which coupled with CFD simulations, will render a powerful tool for digital reactor design.[67] However, these results are the stepping-stone in the development of methodologies bringing together the molecular efficiency, related with the presence of the IL units, and the reactor design for flow process. Besides, the increase in catalytic performance leads to a reduction in waste, since higher yields can be achieved with less amount of catalyst. Thus, these methodologies can contribute to reduce the environmental impact related to the use of ILs by developing complex geometric catalytic devices which optimise conversion and facilitates the separation, recover and reutilization of the catalysts in subsequent reaction cycles.
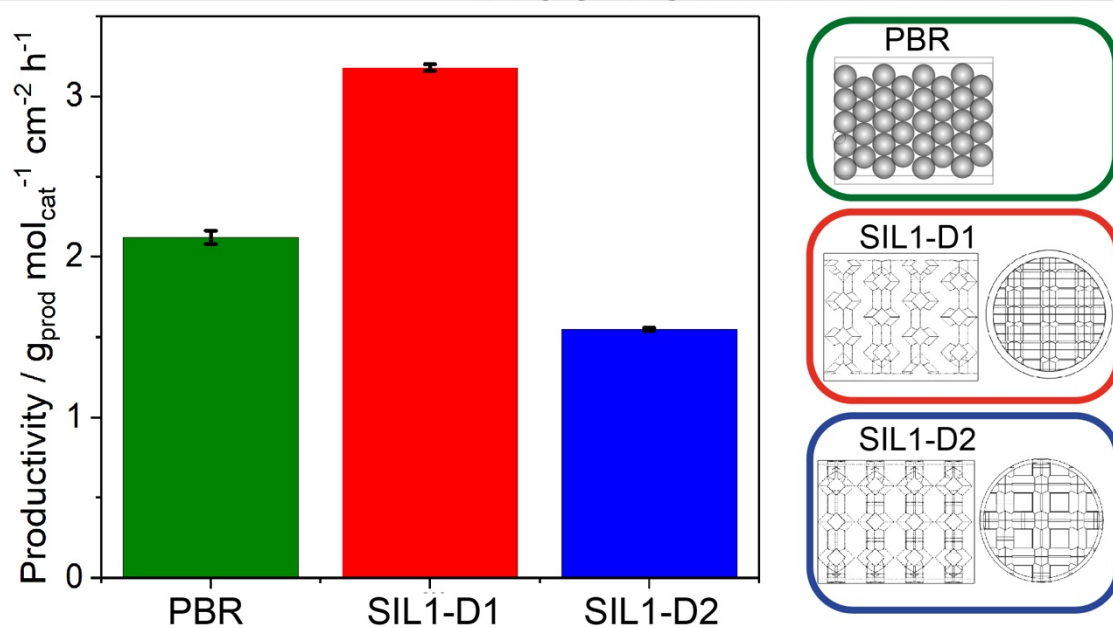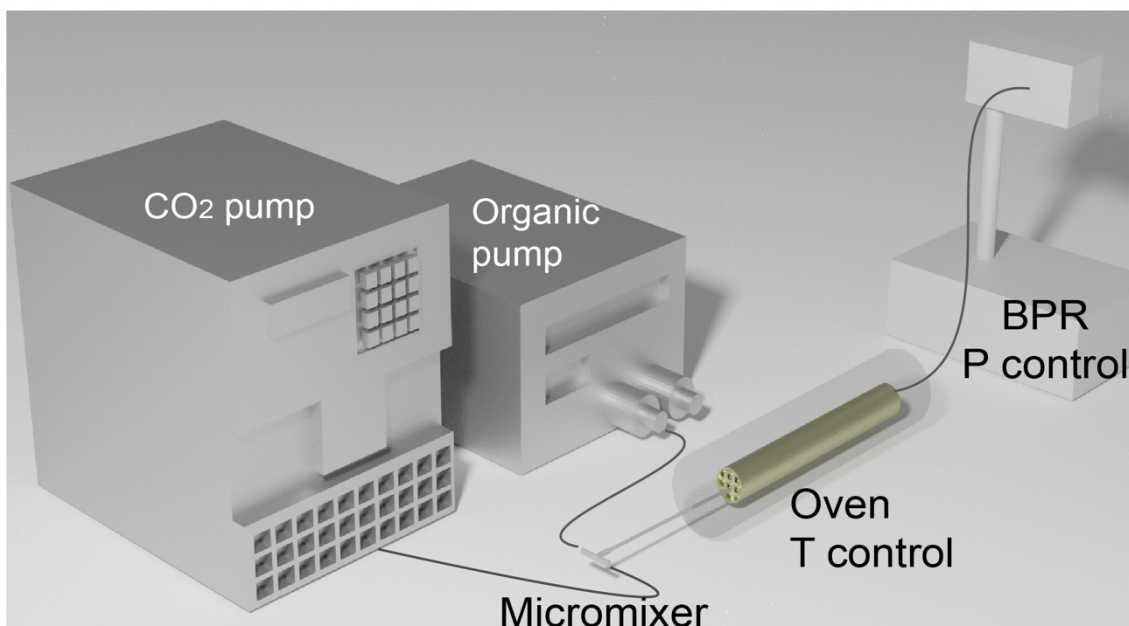
Figure 4. Normalised productivity on stream obtained for the continuous flow reaction between styrene oxide and $CO_2$ at 120 °C and 20 bars. Green: two coupled reactors filled with polymeric beads of P-SIL1 (1.89 g). Red: SIL1-D1 (6.22g with 3.44 mL free volume). Blue: SIL1-D2 (4.45 g with 3.74 mL free volume). Conversion calculated by ^{1}H-NMR. Selectivity > 99%; Productivity ($g_{prod}$ $mol_{cat}^{-1}$ $cm^{-2}$ $h^{-1}$) normalised considering the catalyst loading (determined by elemental analysis) and surface area of material.

With the best catalyst moieties in hands and the best reactor design (**SIL1-D1**), the reactor configuration D1 was fabricated a new formulation with more reactive acrylate-based cross-linkers, shown as the **S2** formulation (entry 17, Table 2). The advantages of this formulation were faster polymerization kinetics (30 s/layer) and it did not require commercial photopolymer resin. The reactor **SIL2-D1** with same active catalyst

moieties than **SIL1-D1** was prepared by reaction of the unmodified epoxy reactor with butyl imidazole in acid media. The FT-IR-ATR and the Raman studies revealed that independently of the crosslinked used the modification of the reactor takes place only on the surface of the polymeric material (Figure S6). Hence, it would be assumed that the backbone formulation plays no role in the catalytic activity. This was validated by comparing the activity of both polymers, which showed similar performance under continuous-flow (Figure S7).

Finally, the temporal stability and substrate scope of the catalytic system was evaluated. In this case, two 10 cm columns were packed in series in SS ¼" columns to facilitate heat transfer during the experiments to easily adapt the experimental conditions to the different substrates assayed. The continuous flow configuration composed by **SIL2-D1** was tested for over 300 h, with no significant loss in activity. Figure 5 shows the yield of cyclic carbonate derivates obtained as a function of the studied substrate and time. Yield of reaction, defined as molar flow rate of product divided by molar flow rate of limiting reagent,[68] was employed here because there is no comparison with other materials or reactor geometries. Three different epoxide substrates have been used and the process conditions were slightly adapted. For the first 50 h of reactor use, styrene oxide (SO) was employed as the reagent, yielding around 80% of product. Following the reactor durability and scope test, the substrate was changed to glycidol (GO), reaching 99% of yield of the correspondent cyclic carbonate during 150 h. Epichlorohydrin (ECH) was used as substrate between 200 and 250 h, with a yield of around 80 % yield of the corresponding product. Finally, SO was employed again for 50 h to demonstrate that the catalyst was maintaining its activity after the different substrates scope. This remarkable result opens a new window of opportunities in flow chemistry, where the combination of SIL-based catalysts and AM, enables the digital design of scalable active reactors according to the desired application.
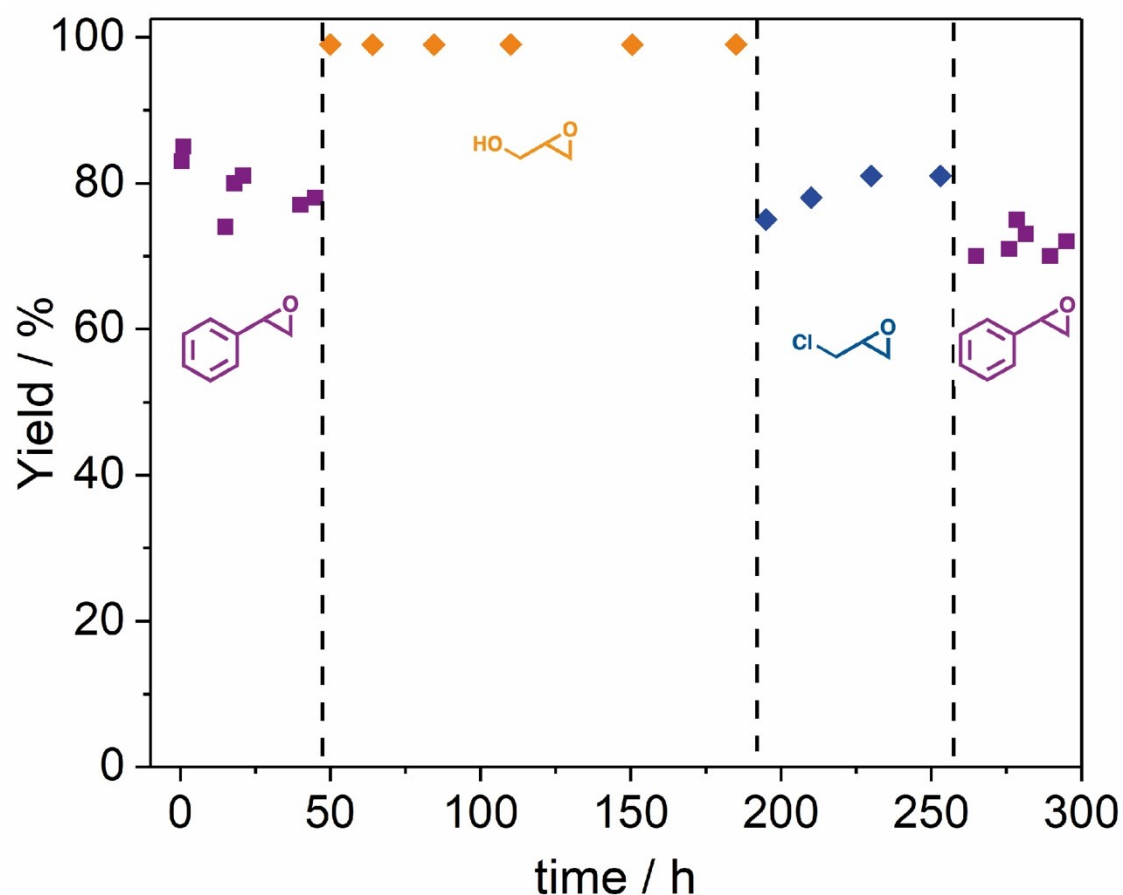
Figure 5. Yield *vs* time on stream obtained for the continuous flow reaction SIL2-D1 between different epoxide and $CO_2$ (65 bar). Purple squares: styrene oxide (SO), reaction performed at 120 ºC. Orange rhombus: glycidol (GO), reaction performed at 90 ºC. Blue rhombus: epichlorohydrin (ECH), reaction performed at 90 ºC. Conversion calculated by $^1$H-NMR. Selectivity > 99%.

## Conclusions

In this work we reported a proof-of-concept of low-footprint continuous flow system for $CO_2$ cycloaddition to epoxides based on SIL 3D printed materials. We have demonstrated that AM manufacturing can be efficiently used to integrate different enabling technologies such as solid phase supported catalysis, flow chemistry and ILs. The preparation and optimisation of an epoxy functionalised ink allowed the preparation of 3D objects, which were post-functionalised with IL-like units to generate catalytic surfaces. The freedom of design provided by AM technology was exploited to design continuous flow reactors with high stability (up 300 h). The catalytic activity observed normalised by the surface area and the catalyst loadings showed for the first-time enhanced activity profiles in comparison to

conventional packed bed reactor configurations at laboratory scale. This suggests that digital reactor design has potential to produced structured reactors with optimal performance and reducing the waste. Furthermore, the increased efficiency allowed to work without solvents, which is an additional advantage in green chemistry point of view. In addition, the new formulation (**SIL2-D1)** demonstrated high productivity and temporal stability of the catalyst with three different epoxide-based substrates. The simple implementation and modification of the reactor design closes the gap between research and industrial application, opening a new avenue of possibilities in $CO_2$ reuse.

## CONFLICTS OF INTEREST

There are no conflicts to declare.

# References

1. E. National Academies of Sciences and Medicine, *Gaseous Carbon Waste Streams Utilization: Status and Research Needs*, The National Academies Press, Washington, DC, 2019.
2. A. Rehman, F. Saleem, F. Javed, A. Ikhlaq, S. W. Ahmad and A. Harvey, *Journal of Environmental Chemical Engineering*, 2021, **9**, 105113-105113.
3. Q.-W. Song, Z.-H. Zhou and L.-N. He, *Green Chemistry*, 2017, **19**, 3707-3728.
4. L. Guo, K. J. Lamb and M. North, *Green Chemistry*, 2021, **23**, 77-118.
5. D. Rigo, R. Calmanti, A. Perosa, M. Selva and G. Fiorani, *ChemCatChem*, 2021, **13**, 2005-2016.
6. D. Valverde, R. Porcar, P. Lozano, E. García-Verdugo and S. V. Luis, *ACS Sustainable Chemistry & Engineering*, 2021, **9**, 2309-2318.
7. H. Seo, L. V. Nguyen and T. F. Jamison, *Advanced Synthesis & Catalysis*, 2019, **361**, 247-264.

8.  N. Zanda, A. Sobolewska, E. Alza, A. W. Kleij and M. A. Pericàs, *ACS Sustainable Chemistry & Engineering*, 2021, **9**, 4391-4397.
9.  J. A. Kozak, J. Wu, X. Su, F. Simeon, T. A. Hatton and T. F. Jamison, *Journal of the American Chemical Society*, 2013, **135**, 18497-18501.
10. S. G. Newman and K. F. Jensen, *Green Chemistry*, 2013, **15**, 1456-1472.
11. E. García-Verdugo, B. Altava, M. I. Burguete, P. Lozano and S. V. Luis, *Green Chem.*, 2015, **17**, 2693-2713.
12. R. Gérardy, J. Estager, P. Luis, D. P. Debecker and J.-C. M. Monbaliu, *Catalysis Science & Technology*, 2019, **9**, 6841-6851.
13. F. Ferlin, D. Lanari and L. Vaccaro, *Green Chemistry*, 2020, **22**, 5937-5955.
14. O. Levenspiel, *Industrial & Engineering Chemistry Research*, 1999, **38**, 4140-4143.
15. W. E. Frazier, *Journal of Materials Engineering and Performance*, 2014, **23**, 1917-1928.
16. S. C. Ligon, R. Liska, J. Stampfl, M. Gurr and R. Mülhaupt, *Chemical Reviews*, 2017, **117**, 10212-10290.
17. M. R. Hartings and Z. Ahmed, *Nature Reviews Chemistry*, 2019, **3**, 305-314.
18. O. Okafor, A. Weilhard, J. A. Fernandes, E. Karjalainen, R. Goodridge and V. Sans, *Reaction Chemistry & Engineering*, 2017, **2**, 129-136.
19. D. A. Walker, J. L. Hedrick and C. A. Mirkin, *Science*, 2019, **366**, 360-364.
20. E. Peris, O. Okafor, E. Kulcinskaja, R. Goodridge, S. V. Luis, E. Garcia-Verdugo, E. O'Reilly and V. Sans, *Green Chem.*, 2017, **19**, 5345-5349.
21. V. Sans, *Current Opinion in Green and Sustainable Chemistry*, 2020, **25**, 100367-100367.
22. S. Rossi, A. Puglisi and M. Benaglia, *ChemCatChem*, 2018, **10**, 1512-1525.
23. V. Dragone, V. Sans, M. H. Rosnes, P. J. Kitson and L. Cronin, *Beilstein J. Org. Chem*, 2013, **9**, 951-959.
24. P. J. Kitson, M. H. Rosnes, V. Sans, V. Dragone and L. Cronin, *Lab on a Chip*, 2012, **12**, 3267-3271.
25. B. Gutmann, M. Köckinger, G. Glotz, T. Ciaglia, E. Slama, M. Zadravec, S. Pfanner, M. C. Maier, H. Gruber-Wölfler and C. Oliver Kappe, *Reaction Chemistry & Engineering*, 2017, **2**, 919-927.
26. Z.-J. Li, J.-F. Sun, Q.-Q. Xu and J.-Z. Yin, *ChemCatChem*, 2021, **13**, 1848-1866.
27. A. A. Chaugule, A. H. Tamboli and H. Kim, *Fuel*, 2017, **200**, 316-332.
28. V. Sans, N. Karbass, M. I. Burguete, V. Compañ, E. García-Verdugo, S. V. Luis and M. Pawlak, *Chemistry – A European Journal*, 2011, **17**, 1894-1906.
29. S. Montolio, B. Altava, E. García-Verdugo and S. V. Luis, in *Green Synthetic Processes and Procedures*, The Royal Society of Chemistry, 2019, DOI: 10.1039/9781788016131-00289, pp. 289-318.
30. F. Giacalone and M. Gruttadauria, *ChemCatChem*, 2016, **8**, 664-684.
31. D. J. Wales, Q. Cao, K. Kastner, E. Karjalainen, G. N. Newton and V. Sans, *Advanced Materials*, 2018, **30**, 1800159.
32. D. J. Wales, S. Miralles-Comins, I. Franco-Castillo, J. M. Cameron, Q. Cao, E. Karjalainen, J. Alves Fernandes, G. N. Newton, S. G. Mitchell and V. Sans, *Biomaterials Science*, 2021, **9**, 5397-5406.
33. H. Nulwala, A. Mirjafari and X. Zhou, *European Polymer Journal*, 2018, **108**, 390-398.
34. A. S. Martinez, C. Hauzenberger, A. R. Sahoo, Z. Csendes, H. Hoffmann and K. Bica, *Acs Sustainable Chemistry & Engineering*, 2018, **6**, 13131-13139.
35. A. Weiß, M. Munoz, A. Haas, F. Rietzler, H.-P. Steinrück, M. Haumann, P. Wasserscheid and B. J. M. Etzold, *ACS Catalysis*, 2016, **6**, 2280-2286.
36. M. J. Schneider, M. Lijewski, R. Woelfel, M. Haumann and P. Wasserscheid, *Angewandte Chemie International Edition*, 2013, **52**, 6996-6999.

37. M. Hatanaka, T. Yasuda, E. Uchiage, M. Nishida and K.-i. Tominaga, *ACS Sustainable Chemistry & Engineering*, 2021, **9**, 11674-11680.
38. D. Geier, P. Schmitz, J. Walkowiak, W. Leitner and G. Franciò, *ACS Catalysis*, 2018, **8**, 3297-3303.
39. T. Wang, W. Wang, Y. Lyu, X. Chen, C. Li, Y. Zhang, X. Song and Y. Ding, *RSC Advances*, 2017, **7**, 2836-2841.
40. S. El Sayed, A. Bordet, C. Weidenthaler, W. Hetaba, K. L. Luska and W. Leitner, *ACS Catalysis*, 2020, **10**, 2124-2130.
41. J. Kalal, F. Švec and V. Maroušek, *Journal of Polymer Science: Polymer Symposia*, 1974, **47**, 155-166.
42. Ezzah M. Muzammil, A. Khan and M. C. Stuparu, *RSC Advances*, 2017, **7**, 55874-55884.
43. D. C. Sherrington, *Chemical Communications*, 1998, DOI: 10.1039/A803757D, 2275-2286.
44. V. Sans, N. Karbass, M. I. Burguete, E. García-Verdugo and S. V. Luis, *RSC Advances*, 2012, **2**, 8721-8728.
45. T. Zhu, W. Bi and K. H. Row, *Journal of Applied Polymer Science*, 2010, **118**, 3425-3430.
46. V. H. Paschoal, L. F. O. Faria and M. C. C. Ribeiro, *Chemical Reviews*, 2017, **117**, 7053-7112.
47. F. M. Mirabella, *Internal Reflection Spectroscopy - Theory and Applications* CRC Press, 1993.
48. D. Y. Zhu, G. S. Cao, W. L. Qiu, M. Z. Rong and M. Q. Zhang, *Polymer*, 2015, **69**, 1-9.
49. T. Yamada, Y. Tominari, S. Tanaka and M. Mizuno, *The Journal of Physical Chemistry B*, 2017, **121**, 3121-3129.
50. Y. Dong, J. Li, L. Shi, X. Wang, Z. Guo and W. Liu, *Chemical Communications*, 2014, **50**, 5586-5589.
51. Y. Zhao, M. Li and Q. Lu, *Langmuir*, 2008, **24**, 3937-3943.
52. B.-S. Ta - Lee and S. K. Ta - Rhee, *Bulletin of the Korean Chemical Society*, 2004, **25**, 1531-1537.
53. B. S. Lee, Y. S. Chi, J. K. Lee, I. S. Choi, C. E. Song, S. K. Namgoong and S.-g. Lee, *Journal of the American Chemical Society*, 2004, **126**, 480-481.
54. X. He, W. Yang and X. Pei, *Macromolecules*, 2008, **41**, 4615-4621.
55. B. Xin and J. Hao, *RSC Advances*, 2012, **2**, 5141-5146.
56. A.-L. Girard, N. Simon, M. Zanatta, S. Marmitt, P. Gonçalves and J. Dupont, *Green Chem.*, 2014, **16**, 2815-2825.
57. T.-Y. Shi, J.-Q. Wang, J. Sun, M.-H. Wang, W.-G. Cheng and S.-J. Zhang, *RSC Advances*, 2013, **3**, 3726-3732.
58. M. Cokoja, M. E. Wilhelm, M. H. Anthofer, W. A. Herrmann and F. E. Kühn, *ChemSusChem*, 2015, **8**, 2436-2454.
59. J. Zhang, X. Li, Z. Zhu, T. Chang, X. Fu, Y. Hao, X. Meng, B. Panchal and S. Qin, *Advanced Sustainable Systems*, 2021, **5**, 1-8.
60. H. Kawanami, A. Sasaki, K. Matsui and Y. Ikushima, *Chemical Communications*, 2003, DOI: 10.1039/B212823C, 896-897.
61. A. Dani, E. Groppo, C. Barolo, J. G. Vitillo and S. Bordiga, *Journal of Materials Chemistry A*, 2015, **3**, 8508-8518.
62. D. Valverde, R. Porcar, P. Lozano, E. García-Verdugo and S. V. Luis, *ACS Sustainable Chemistry and Engineering*, 2021, **9**, 2309-2318.
63. R. K. Tak, P. Patel, S. Subramanian, R. I. Kureshy and N.-u. H. Khan, *ACS Sustainable Chemistry & Engineering*, 2018, **6**, 11200-11205.
64. A. L. Girard, N. Simon, M. Zanatta, S. Marmitt, P. Gonçalves and J. Dupont, *Green Chemistry*, 2014, **16**, 2815-2825.

65.    Y. He, D. Jiang, X. Li, J. Ding, H. Li, H. Wan and G. Guan, *Journal of CO2 Utilization*, 2021, **44**, 101427-101427.

66.    H. Gou, X. Ma, Q. Su, L. Liu, T. Ying, W. Qian, L. Dong and W. Cheng, *Physical Chemistry Chemical Physics*, 2021, **23**, 2005-2014.

67.    E. Alvarez, M. Romero-Fernandez, D. Iglesias, R. Martinez-Cuenca, O. Okafor, A. Delorme, P. Lozano, R. Goodridge, F. Paradisi, D. A. Walsh and V. Sans, *ACS Sustainable Chemistry & Engineering*, 2022, **10**, 2388-2396.

68.    H. S. Fogler, *Elements of chemical reaction engineering*, Third edition. Upper Saddle River, N.J. : Prentice Hall PTR, 1999.

Table of Contents

SIL

Catalysis

3DP